agronomy

MDPI

Article

Open-Field Agrivoltaic System Impacts on Photothermal Environment and Light Environment Simulation Analysis in Eastern China

Long Zhang [1,2], Zhipeng Yang [3], Xue Wu [2], Wenju Wang [4], Chen Yang [5], Guijun Xu [5], Cuinan Wu [2,*] and Encai Bao [1,2,*]

[1] School of Agricultural Engineering, Jiangsu University, Zhenjiang 212013, China
[2] Institute of Agricultural Facilities and Equipment, Jiangsu Academy of Agricultural Sciences, Nanjing 210014, China
[3] School of Engineering, Anhui Agricultural University, Hefei 230036, China
[4] School of Energy and Power Engineering, Nanjing University of Science and Technology, Nanjing 210094, China; wangwenju1982@163.com
[5] Shenzhen Energy Nanjing Holding Co., Ltd., Nanjing 210019, China
* Correspondence: wucuinan@126.com (C.W.); baoencai1990@163.com (E.B.); Tel.: +86-159-5188-7596 (C.W.); +86-177-6810-3527 (E.B.)

Abstract: In order to clarify the temporal and spatial changes in the internal photothermal environment in an open-field agrivoltaic system (OAVS), this paper took the OAVS in eastern China as the research object and divided the internal area into the southern area, middle area and northern area, according to the spatial structure. Further, a photothermal environment test was conducted in the above three areas in the summer and winter. The results showed that the summer average daylight rate ($R_{m\text{-}avg}$) in the middle area was 66.6%, while the $R_{m\text{-}avg}$ in the other two areas was about 20%, with no significant difference. In the winter, the light environment in the southern area was slightly better, and the $R_{m\text{-}avg}$ in the above three areas was 26.4%, 24.7% and 19.7%, respectively. On the whole, the relationship between the thermal environmental factors and the solar radiation intensity was consistent. Further, a 3D model of an OAVS was established using Autodesk Ecotect Analysis 2011, and the internal light environment was simulated. Compared with the measured values, the relative error was less than 10%, which verified the reliability of the OAVS model. Then, the model was used to reveal the temporal and spatial changes in the light environment of the OAVS. The simulation results showed that the daylighting rate in the summer from the ground to the height of the fig canopy inside the system was 20.7% to 61.5%. In the winter, the daylighting rate from the ground to the height of the fig canopy inside the system was 17.7% to 36.4%. The effectiveness of the OAVS in reducing the level of solar radiation intensity depended on the time of day and the angle of the sun. At the spatial scale, due to the strong consumption of light by photovoltaic panels, there was a strong horizontal and vertical light environment gradient inside the system. In conclusion, the photothermal environment research of an OAVS based on Autodesk Ecotect Analysis 2011 can not only provide a basis for agricultural production and structural design such as span, height and the laying density of PV panels, but also expand its application to regions with different latitudes and longitudes and specific climates.

Keywords: agrivoltaics; agricultural building; photothermal environment; ECOTECT; simulation

Citation: Zhang, L.; Yang, Z.; Wu, X.; Wang, W.; Yang, C.; Xu, G.; Wu, C.; Bao, E. Open-Field Agrivoltaic System Impacts on Photothermal Environment and Light Environment Simulation Analysis in Eastern China. *Agronomy* **2023**, *13*, 1820. https://doi.org/10.3390/agronomy13071820

Academic Editors: Xiongkui He, Fuzeng Yang and Baijing Qiu

Received: 12 June 2023
Revised: 3 July 2023
Accepted: 5 July 2023
Published: 8 July 2023

1. Introduction

The open-field agrivoltaic system (OAVS) is a modern integrated agricultural production system which combines PV power generation and agricultural production [1,2]. Under the condition that agricultural land and agricultural production are not affected, it can improve the efficiency of land use, which is of great significance to the development

of the PV industry and the transformation of modern agriculture [3,4]. In the context of carbon neutrality, the development and utilization of solar energy has become an important "tuyere" [5]. The OAVS has been widely applied and promoted in China, which combines PV and field planting [6]. Relying on a good agricultural resource base, the OAVS project has developed rapidly in eastern China [7]. By the end of 2022, the cumulative grid-connected capacity of centralized PV power stations in this area reached 72.96 million kW, accounting for 19.8% of the national grid-connected capacity, among which the OAVS is the main application form of centralized PV power stations in this area [8]. At the same time, this area is the main vegetable-producing area in China, and has great potential for agrivoltaic implementation [9]. For example, the installed PV-saturated capacity of Jiangsu Province and Shandong Province in eastern China can reach 18.25 GW and 16.00 GW, respectively [7]. At present, the OAVS in East China covers a large area and is relatively concentrated in scale, making it easy to carry out large-scale, mechanized and intensive agricultural production. However, affected by the occlusion of photovoltaic panels, the OAVS is conducive to the growth and development of shad-tolerant and cold-loving crops [10]. Therefore, the OAVS is mostly planted with shad-tolerant, compact, high yield and high efficiency crop types and varieties. For example, it is suitable to plant corn, sorghum, potato, taro, yam and beans between the boards and under the eaves, and shady crops such as Chinese medicinal materials can be planted under the columns [11–14].

The development of the OAVS project can improve land utilization rate [15,16], promote industrial low carbon development [17,18], enrich field biomass [19], improve soil moisture [19,20] and increase comprehensive benefits [21,22]. However, there are some tricky problems in the OAVS in this area, such as the unclear internal photothermal environment and the poor coupling effect of agriculture and PV [23]. A large number of studies have shown that due to the shading of PV panels, there are phenomena such as uneven distribution and low intensity of light inside the system, which affect the normal growth of crops [24,25]. In order to clarify the variation rule in the internal photothermal environment of the OAVS, experts and scholars at home and abroad have conducted a lot of research on the photothermal environment of the system and similar PV buildings. Marrou et al. [26] monitored the microclimatic conditions of different PV panel laying densities in the OAVS in different seasons. The results showed that there was no significant difference in average daily air temperature and average daily relative humidity under different treatments, but there was a gradient difference in soil temperature. Gao et al. [27] studied the diurnal and annual variation characteristics of air temperature inside and outside of PV power stations. Through monitoring and the analysis of a single point inside and outside the power station, the results showed that the daytime air temperature inside and outside the power station was basically the same in the winter. In the spring, summer and autumn, the air temperature inside the power station was significantly higher than that outside, and the difference was the largest in the summer, 0.67 °C. Hassanpour Adeh et al. [19] studied the environmental effects of PV panels on unirrigated grasslands that frequently suffer from water stress, quantifying the effects of the presence of PV panels on microclimate and soil moisture. The results showed that the area under the PV panel maintained a higher soil moisture, and the biomass increased by 90% in the later period. Chang et al. [28] studied the thermal effect of PV panels on the temperature of adjacent air, and the results showed that the temperature of PV panels (height of the erection was 2 m) increased significantly, with an average annual increase of 9.7 °C and an average annual increase in adjacent air temperature of 3.8 °C. Sailor et al. [29] found through research that PV urban building systems heat the city during the day and cool it at night. Ezzaeri et al. [30] studied the effects of checkerboard form flexible PV panels on greenhouse microclimates and tomato yields in the summer and winter. The results showed that the PV panel reduced the air temperature in the greenhouse, and the occupancy rate of PV panel had no significant effect on the total yield of tomato.

In summary, the internal environment of the OAVS is relatively complex and has an important impact on agricultural production. However, there are no reports on the

variation rule of the photothermal environment inside the system at a spatial scale. It is an important basis for the agricultural production of the OAVS to make clear the variation rule of internal environment and the photothermal performance. The accurate photothermal environment can not only provide a basis for the OAVS agricultural mode selection and production management, but also provide reference for the structural design of the system span, height and PV panel laying density.

As a civil building software, Autodesk Ecotect Analysis 2011 is able to conduct light environment analysis, energy consumption analysis and sunshine and shade analysis for buildings by setting building structural parameters, material parameters and environmental parameters [31–33]. Various studies show that the simulation accuracy of the software is good [34,35]. When applying the software for research and analysis, the boundary conditions are convenient to set, the operation process is relatively simple and the result visualization ability is strong [36,37]. Although the software is mainly used for the analysis of civil buildings, it has a broad prospect in the analysis and application of the light environment of agricultural buildings.

This paper will take the OAVS in eastern China as the research object and measure the solar radiation intensity, air temperature and soil temperature in the summer and winter. Further, the distribution of environmental parameters in different areas will be analyzed. Combined with Autodesk Ecotect Analysis 2011, a proportional agrivoltaic system model will be constructed to simulate and analyze the solar radiation, shading and sunshine hours in the system, so as to clarify its optical environment performance in space and time scales. The novelties of this study are as follows: (1) Combined with the sensor configuration strategy and spatial structure characteristics, the change rule of the photothermal environment in different areas inside the OAVS in the summer and winter is quantified. (2) The OAVS light environment model is established, revealing the spatial and temporal scales system interior light environment distribution characteristics.

2. Materials and Methods

2.1. Experimental Site Description

The experimental OAVS is located in Shenzhen Energy Nanjing Holding Co., Ltd. (31.62° latitude, 119.18° longitude, approx. 360 m above sea level), Lishui District, Nanjing City, Jiangsu Province, China. The power station was put into operation in 2016, covering an area of about 46.67 ha, with a total installed capacity of 20 MW and annual clean power generation of about 24 million kWh. It is also a base integrating photovoltaic power generation, ecological agriculture, sightseeing tourism, popular science exhibition and photovoltaic agricultural research and experiment (Figure 1a). Lishui district is in the transition zone from the north subtropical zone to the middle subtropical zone. The average annual temperature is 15.5 °C. The average annual sunshine duration is 2145.8 h and the average annual rainfall is 1036.9 mm.

The PV panels of the system face south and are supported by Φ300 concrete piles and an inclined supporting frame. The distance between concrete piles is 3 m and 6.8 m between the panel arrays. The PV module is made of 265 W polysilicon, with a photoelectric conversion efficiency of 16.3%. The size of a single PV module is 1640 × 992 × 35 mm, composed of 60 minimum cells. Four PV modules are arranged in a row and continuously laid along the east–west direction. The lowest edge of the PV modules is 3.2 m above the ground and has a tilt angle of 24°. One row of fig (*Ficus carica*) trees were planted in the middle of each span in the OAVS with a height of about 1.0 m and a root length of about 0.3 m. The figs were equally spaced with planting spacing of about 3.0 m, and their main growing season at this site is from April to October. The soil texture is classified as yellow loam. In addition, since the PV panes have the function of collecting rain, two drainage ditches in the east–west direction are formed inside the single span PV array (Figure 1b,c).

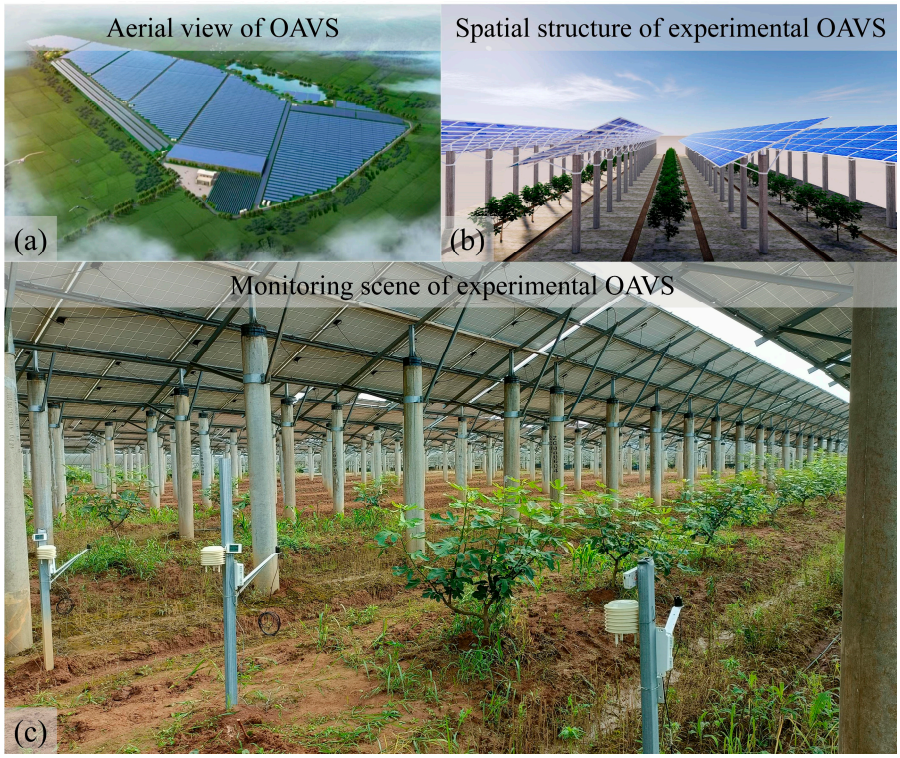

Figure 1. (**a**) Aerial view of OAVS; (**b**) spatial structure of experimental OAVS; (**c**) monitoring points in experimental OAVS.

2.2. Photothermal Environment Measurement and Daylighting Rate Calculation

According to the needs of the experimental design, the space occupied by the PV arrays is defined as the interior of the OAVS. The height of the space is the lowest height of the PV panel from the ground, which is about 3.2 m. The exterior of the OAVS is defined as a place far away from the OAVS and sufficiently open. According to the spatial structure of the OAVS, the single span PV array was divided into three areas along the north–south direction, namely, southern area, middle area and northern area. The width of each area is 1.8, 3.2 and 1.8 m, respectively (Figure 2). The environmental factors monitored inside and outside of this experimental OAVS include solar radiation intensity, air temperature and soil temperature. The arrangement of monitoring instruments in the three areas follows the following principles: (1) Reduce the sensor configuration redundancy under the condition of meeting the information collection requirements; (2) fully consider the shading of photovoltaic modules, plant height, plant root length and other factors; the expected test results can fully reflect the objective law to avoid a bad impact on the monitoring of the light temperature sensor. Based on this, the solar radiation intensity and air temperature measurement point was set at 1.0 m above the ground, the same as the height of the fig tree canopy, and the soil temperature measurement point was set at 0.15 m underground, which was in the middle position of fig root depth. The instruments were arranged 0.65 m away from the axis of the prefabricated pipe pile to fully reflect the photothermal performance of the OAVS.

The arrangement of measuring points is shown in Figure 2: (1) Solar radiation intensity and air temperature in the OAVS: Sensors for solar radiation intensity and air temperature were placed at south area, middle area and north area, respectively, which were 0.65, 3.40 and 6.15 m away from the concrete pile along the north–south direction and 1.0 m above the ground, one sensor for each area. (2) Soil temperature in the OAVS: Soil temperature measuring sensors were placed at depth of 0.15 m directly below the solar radiation intensity and air temperature measuring points, one sensor for each area. (3) All the measuring points of solar radiation intensity, air temperature and soil temperature inside the OAVS were arranged in the same plane along the north–south direction, and were not affected by side

light. (4) The OAVS external environment measuring point: An environmental measuring point was set in open field far away from the PV arrays. The data of solar radiation intensity at a height of 1.0 m above the ground, air temperature and soil temperature at a depth of 0.15 m were collected. The monitoring scene of the experimental OAVS is shown in Figure 1c.

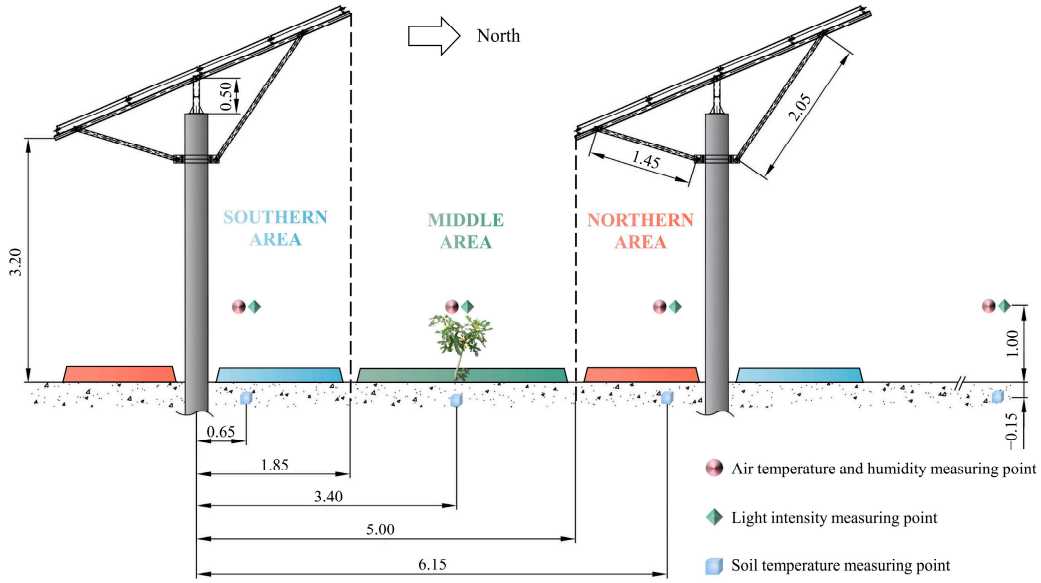

Figure 2. Layout of measuring points inside and outside the experimental OAVS.

Data were collected in the summer from 11 August 2022 to 25 August 2022 and in the winter from 15 December 2022 to 30 December 2022. The test instruments were HOBO series sensors, as shown in Table 1. The environmental data were recorded throughout the day at 30 min intervals. The HOBO UX100-011A air temperature sensor was equipped with a special meteorological radiation shield to eliminate the effects of solar radiation and complex outdoor environment on data reliability. The daytime period in the summer and winter was calculated from 06:00 to 18:00, and the night period was from 18:00 to 06:00^{+1}.

Table 1. Instrument parameters.

Instrument Name	Manufacturer	Model	Range	Accuracy
HOBO temperature recorder	Onset Co., Ltd., Bourne, MA, USA	UX100-011A	−20~+70 °C	±0.2 °C
HOBO four-channel recorder		UX120-006M	−20~+70 °C	±0.2 °C
HOBO temperature sensor		TMC20-HD	−20~+100 °C	±0.15 °C
HOBO total solar radiation sensor		S-LIB-M003	0~+1280 W/m^2	±10 W/m^2

Daylighting rate, as a key evaluation index, was used in the analysis of the light environment of various buildings [38,39]. Sun et al. [40] took the ratio of the average solar radiation intensity inside the greenhouse and outdoor in a single moment as the average daylighting rate to evaluate the lighting performance of the greenhouse. Based on this, the ratio of the average daily internal solar radiation intensity ($E_{m\text{-}in}$) to the average daily outdoor solar radiation intensity ($E_{m\text{-}out}$) is prescribed in this paper as the daily daylighting rate ($R_{m\text{-}d}$). The average of daily daylighting rate of each measurement point during the whole recording period is described as the average daylighting rate ($R_{m\text{-}avg}$). The $R_{m\text{-}d}$ and $R_{m\text{-}avg}$ are used as the evaluation index of the internal light environment of the OAVS, and calculated according to Equations (1) and (2).

$$R_{m\text{-}d} = \frac{1}{k}\sum_{k=1}^{k} E_{m\text{-}in_k} \Big/ \frac{1}{k}\sum_{k=1}^{k} E_{m\text{-}out_k} \quad (1)$$

$$R_{m\text{-}avg} = \frac{1}{i}\sum_{i=1}^{i} R_{m\text{-}d_i} \quad (2)$$

where $E_{m\text{-}in}$ is the measured value of solar radiation intensity at a single time inside the OAVS (W/m^2); $E_{m\text{-}out}$ is the measured value of solar radiation intensity at a single time outside the OAVS (W/m^2); $R_{m\text{-}d}$ is the daylighting rate of the OAVS (%); $R_{m\text{-}avg}$ is the average daylighting rate (%); k is the number of daily records of solar radiation intensity data; and i is the number of experimental days (d).

2.3. Simulation of Light Environment

The internal photothermal environment of the OAVS is relatively complex according to previous research. Solar radiation intensity is the primary ecological factor in the OAVS and has strong interaction effects with other environmental factors. Therefore, Autodesk Ecotect Analysis 2011 was used to construct the light environment model of the OAVS to clarify the light environment performance in both spatial and temporal scales.

2.3.1. Model Construction

The 1:1 OAVS model (Figure 3) was established through a 3D framework (SOLIDWORKS 2020, France) and imported into Autodesk Ecotect Analysis 2011. The typical annual weather data of Nanjing was adopted, and relevant data were put into ECOTECT weather tools to automatically extract meteorological conditions such as direct/scattered solar radiation, annual temperature/humidity variation and annual wind speed variation. Then, the shading rate, sunlight hours and solar radiation inside the OAVS were elaborated based on the actual orientation and inclination. Building material attributes are not included in this paper, as solar radiation and other studied indicators are mainly related to solar altitude angle and azimuth angle. A flowchart for the OAVS simulation procedure was designed based on the model as shown in Figure 4.

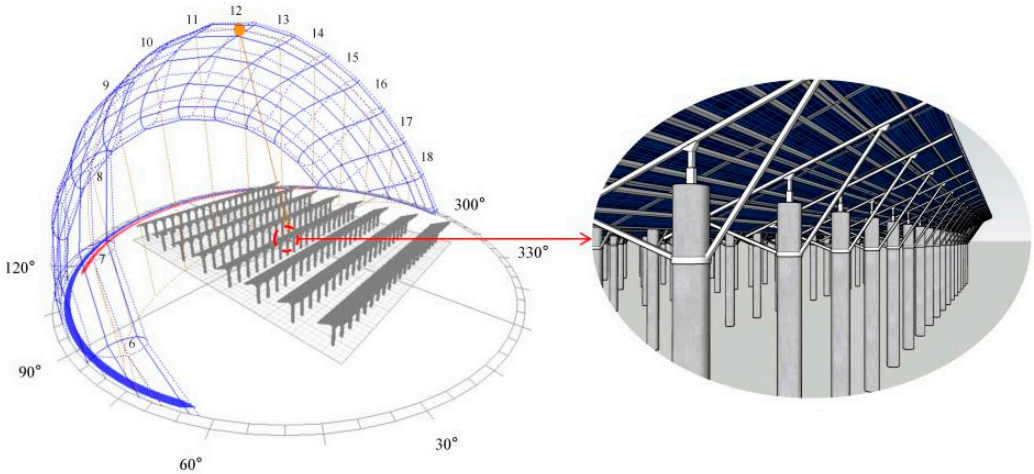

Figure 3. ECOTECT model of OAVS. "6-18"shows the hours of a day.

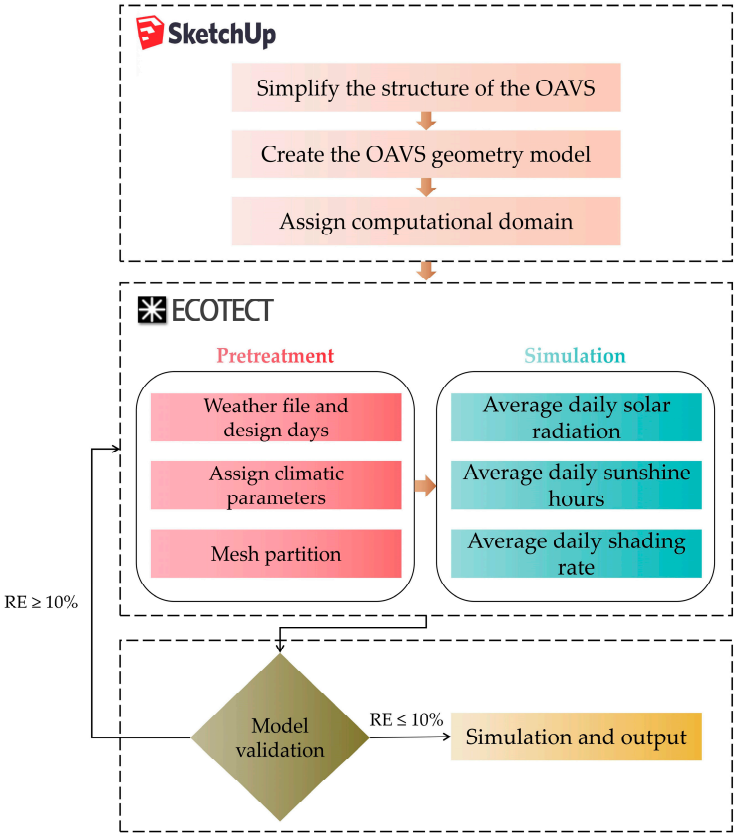

Figure 4. Flowchart for OAVS simulation procedure.

2.3.2. Setting of Numerical Simulation

The center area of the PV arrays was chosen as the calculation domain to eliminate the effect of side light. During grid division, the east–west profile was selected as the simulation plane, and the simulation plane was divided into grid units and calculated in turn. The "display analysis grid" was selected in the "analysis Grid" panel. The values of "2D slice position" were successively set to the required cross sections for calculation. On the basis of considering calculation accuracy and calculation speed, the mesh density should be increased as much as possible. The number of mesh set in this paper was 2048 ("64 × 32"). In Autodesk Ecotect Analysis 2011, we selected "Solar Access Analysis" in Calculate for relevant simulation settings (Figure 5). The simulated period was consistent with the actual test period.

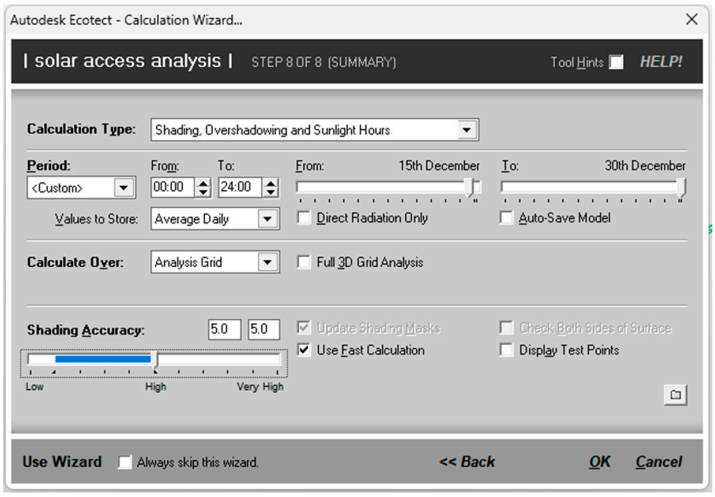

Figure 5. Simulation parameter setting diagram of ECOTET model.

2.4. Data Analysis

Excel 2016 was used for statistical processing and analysis of the experimental data, and Origin 2021 was used to make relevant charts.

3. Results

3.1. Analysis of Photothermal Environment in OAVS

3.1.1. Solar Radiation Intensity

As shown in Figure 6, the solar radiation intensity in the summer and winter differed greatly inside and outside of the OAVS. The solar radiation intensity outside of the OAVS was higher than that of the three measuring points inside the PV arrays. The maximum solar radiation intensity of all the points in the open field, southern area, middle area and northern area in the summer was 391.4, 69.4, 326.3 and 79.0 W/m^2 (Figure 6a), and the maximum solar radiation intensity of all the points in the open field, southern area, middle area and northern area in the winter was 250.3, 170.7, 56.3 and 63.4 W/m^2, respectively (Figure 6b). In the summer, the middle area had the highest solar radiation intensity inside the OAVS, followed by the northern area. The southern area was the lowest. The solar radiation intensity in the OAVS in the winter showed a different change pattern. In the winter, the solar radiation intensity on sunny days in the southern area was higher than that in the other two areas, while on cloudy days, the middle area had the highest solar radiation intensity.

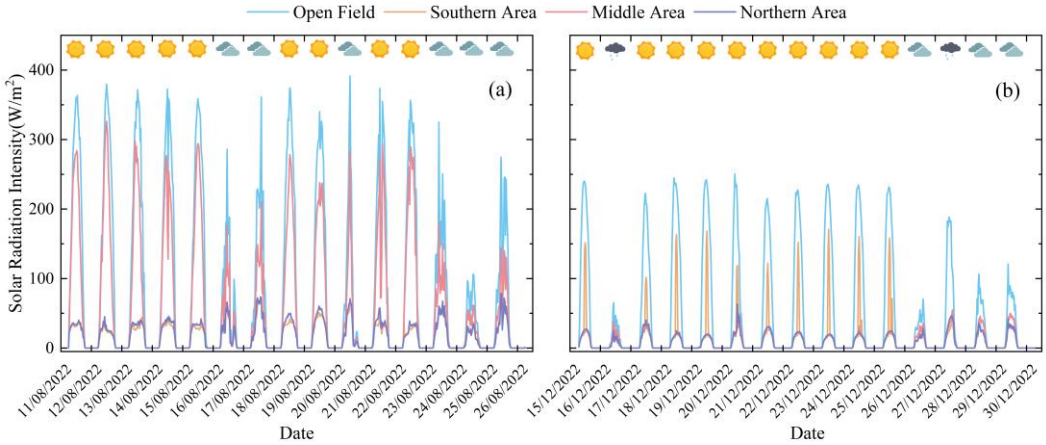

Figure 6. Variation in solar radiation intensity inside and outside OAVS; (**a**) summer; (**b**) winter.

In the summer, on both sunny and cloudy or rainy days, the solar radiation intensity curves of each measuring point had good consistency. On sunny days, the curves first rose from 6 am and reached the highest value at around 12 pm, and then they fell and went back to 0 after 6 pm. The curves of different measuring points reached the peak basically at the same time. On cloudy days, the curves presented more frequent fluctuation, which may be caused by the constant change in cloud thickness, leading to the constant change in direct solar radiation intensity. The change pattern of solar radiation intensity on cloudy days in the winter was similar to that in the summer. However, on sunny winter days, due to the change in solar altitude angle, solar radiation intensity in the southern area increased greatly around 12:00 am, while the other two areas stayed at a lower level.

As shown in Figure 7, the range of $E_{d\text{-}avg}$ in the southern area, middle area and northern area was 53.2~230.7, 18.6~37.3, 31.5~169.8 and 21.6~41.5 W/m^2, respectively. The range of $E_{d\text{-}avg}$ in the winter was 22.3~150.3, 8.7~34.2, 13.0~29.7 and 8.1~23.8 W/m^2, for the southern, middle and northern area, respectively. The $R_{m\text{-}avg}$ in the southern, middle and northern area was 20.5%, 66.6% and 22.7% (summer), and 26.4%, 24.7% and 19.7% (winter), respectively. It can be seen that the $E_{d\text{-}avg}$ and $R_{m\text{-}avg}$ of the OAVS in the summer were the highest in the middle area, and there is no significant difference between the other

two areas. In the winter, the $E_{d\text{-}avg}$ and $R_{m\text{-}avg}$ of the OAVS were larger in the southern area, but the differences among the three areas were relatively small.

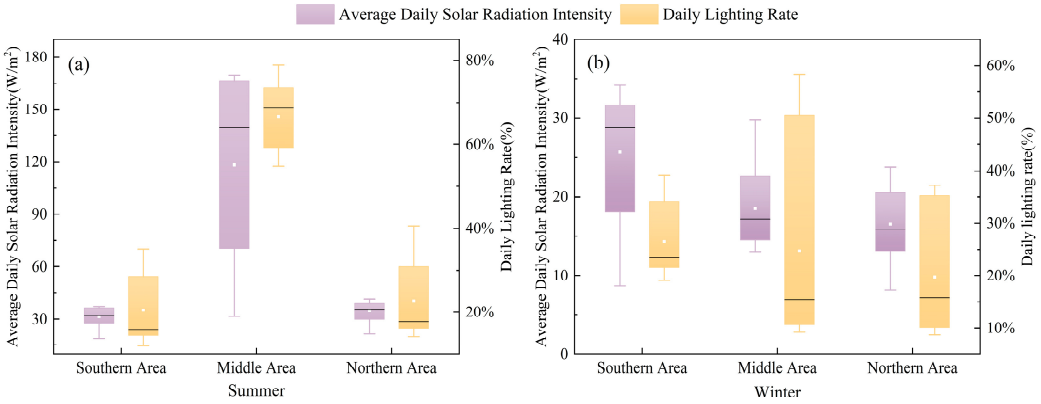

Figure 7. Box plots of average daily solar radiation intensity and daylighting rate in OAVS; (**a**) summer; (**b**) winter.

3.1.2. Air Temperature

Figure 8 shows the changes in air temperature inside and outside of the OAVS in the summer and winter. The statistical data show that the general trend in the air temperature curve inside and outside of the OAVS was basically the same, and the air temperature in the open field was significantly higher than the three measuring points inside the PV array. As shown in Figure 8a, the air temperature of all the measuring points in the open field, southern area, middle area and northern area in the summer ranged from 24.1 °C to 48.7 °C, 24.0 °C to 43.0 °C, 23.9 °C to 48.2 °C and 24.0~47.1 °C. As shown in Figure 8b, the air temperature varied from −8.7 to 16.7 °C, −8.5 to 16.9 °C, −9.0 to 13.7 °C and −8.7 to 14.7 °C at all measuring points in the open field, southern area, middle area and northern area in the winter. In addition, the air temperature distribution curve fluctuated greatly in the two seasons, and the difference between the daily peak value and the daily trough value was obvious, but the regularity was also obvious. In the summer, the air temperature in the three areas of the OAVS was as follows: middle area > northern area > southern area, and the air temperature in the middle area was much higher than that in the other two areas. The variation in air temperature in the three areas of the OAVS in the winter was somewhat different from that in the summer. The overall air temperature in the winter shows that the southern area is higher than the other two areas, and the other two areas are roughly equal.

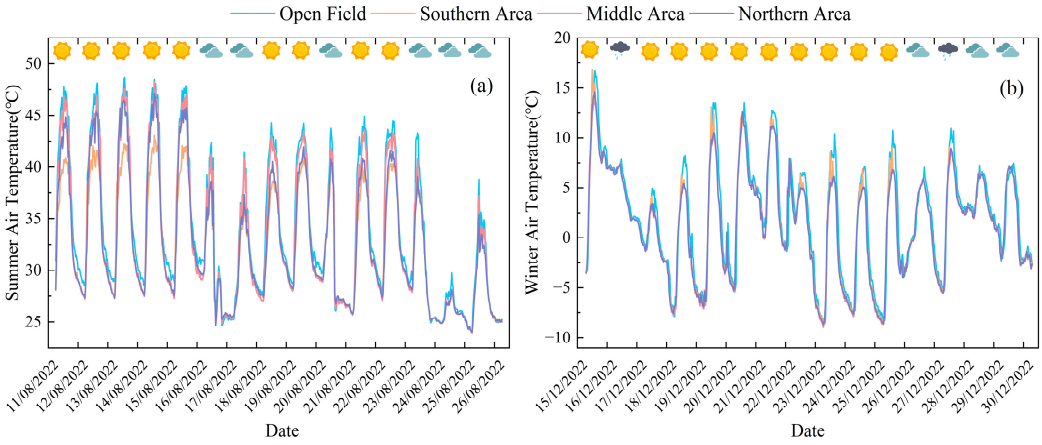

Figure 8. Air temperature variations inside and outside OAVS; (**a**) summer; (**b**) winter.

Combined with the weather types during the two seasons, whether it was sunny or cloudy or rainy, the curves of each measuring point had good consistency, showing a trend

of first rising and then falling, and the corresponding time of peaks of each curve was basically the same. At all measuring points, the temperature basically maintained a gradual rising trend from 06:00 to 12:00, and reached the maximum temperature from 12:00 to 12:00, and gradually dropped from 14:30 to 6:00 the next day.

In order to better display the air temperature differences in different areas of the OAVS, this paper analyzed the distribution of four air temperature parameters. Figure 9 shows the changes in average daily air temperature, average daytime air temperature, average nighttime air temperature and daily extreme air temperature of the OAVS in the summer and winter. In the winter, the above four air temperature indices showed that there was no significant difference among the measuring points inside of the OAVS, and the daytime air temperature of the open field measuring points was slightly higher than that of other measuring points. Taking the average daytime air temperature as an example, the air temperatures in the open field, southern area, middle area and northern area were 5.2 °C, 4.5 °C, 4.2 °C and 4.3 °C, respectively. In the summer, the above three air temperature indices (excluding average nighttime air temperature) all showed the temperature relationship of four measuring points: open field > middle area > northern area > southern area. Taking the average daytime air temperature as an example, the temperature in the above four areas was 38.5 °C, 35.5 °C, 37.6 °C and 36.5 °C, respectively. In addition, there was no significant difference in the average nighttime air temperature at each measuring point in the summer. The air temperature in the above four areas was 29.1 °C, 28.5 °C, 28.4 °C and 28.5 °C, respectively.

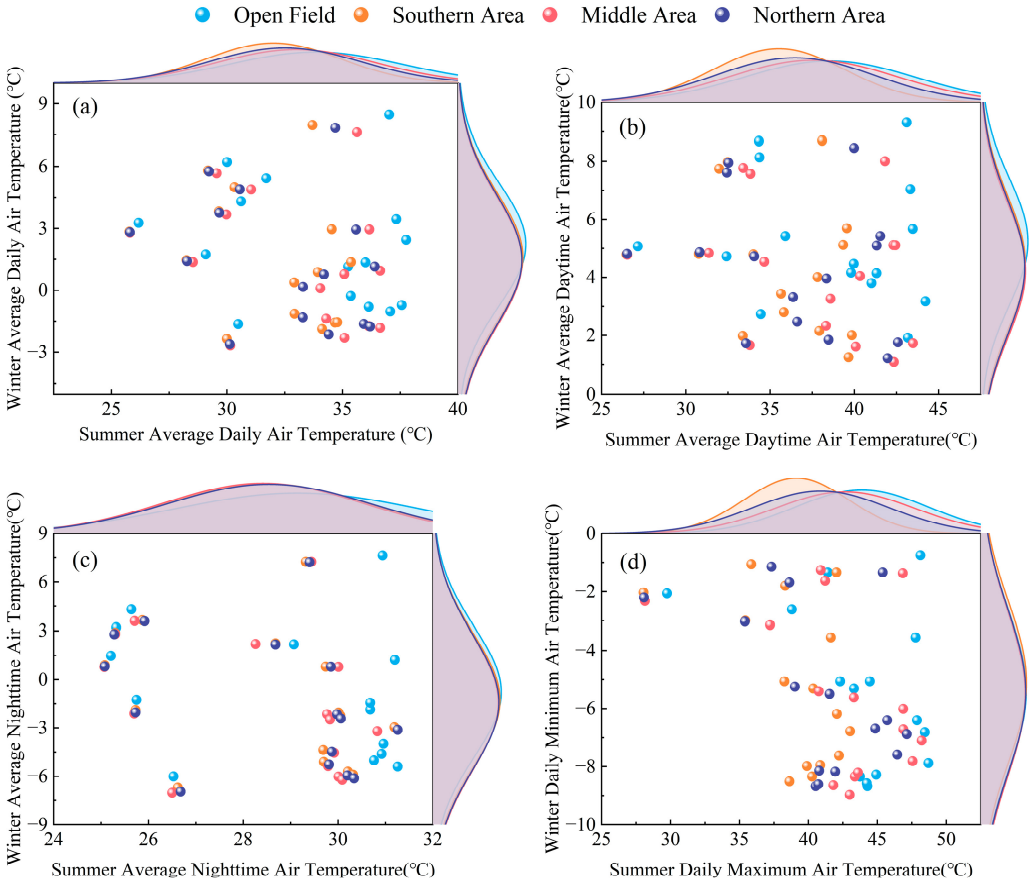

Figure 9. Marginal distribution curve data graph of air temperature in summer and winter; (**a**) average daily air temperature; (**b**) average daytime air temperature; (**c**) average nighttime air temperature; (**d**) daily extreme air temperature.

3.1.3. Soil Temperature

Figure 10 shows the changes in soil temperature inside and outside of the OAVS in the summer and winter. The statistical data show that the soil temperature curves inside and outside of the OAVS had the same general trend, and the soil temperature in the open field was significantly higher than that in the three measuring points inside the PV array. As shown in Figure 10a, the soil temperature of all measuring points in the open field, southern area, middle area and northern area in the summer ranged from 29.4 to 39.6 °C, 26.2 to 36.0 °C, 28.2 to 39.6 °C and 26.7 to 36.2 °C. As shown in Figure 10b, the soil temperature varied from 3.6 to 9.6 °C, 1.9 to 6.8 °C, 1.4 to 6.6 °C and 1.6 to 6.5 °C at all measuring points in the open field, southern area, middle area and northern area in the winter. In addition, the soil temperature distribution curve fluctuated greatly in the two seasons, and the difference between the daily peak value and the daily trough value in the four areas was obvious, but the regularity was also obvious. The relationship of soil temperature in the three areas of the OAVS in the summer was as follows: middle area > northern area > southern area, and the soil temperature in the middle area was much greater than that in the other two areas. In the winter, the soil temperature in the three areas of the OAVS was different from that in the summer. The soil temperature in middle area was greater than that in the southern area and the northern area, and the soil temperature in the southern and northern areas was roughly equal.

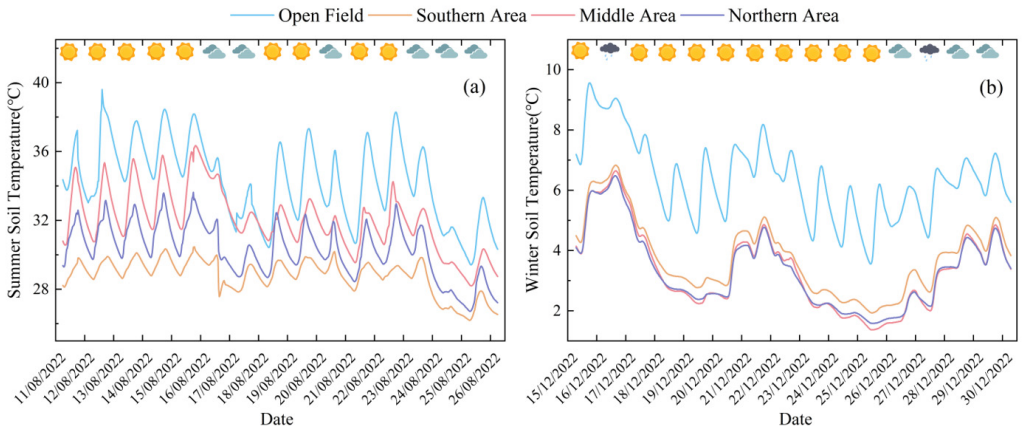

Figure 10. Soil temperature variations inside and outside OAVS; (**a**) summer; (**b**) winter.

Combined with the weather types during the two seasons, whether it was sunny or cloudy or rainy, the curves of each measuring point had good consistency, showing a trend of first rising and then falling, and the corresponding time of peaks of each curve was basically the same. All soil temperature measurement points basically maintained a gradually rising trend during the day, reached the maximum value at sunset and gradually decreased at night.

In order to better display the soil temperature differences in different areas of the OAVS, this paper analyzed the distribution of four soil temperature parameters. Figure 11 shows the variation in average daily soil temperature, average daytime soil temperature, average nighttime soil temperature and daily extreme soil temperature of the OAVS in the summer and winter, and the variation in each index was obvious. In the summer, the above four soil temperature indices all show the relationship between soil temperature in four areas: open field > middle area > northern area > southern area. Taking the average daytime soil temperature as an example, the average daytime soil temperature in the open field, southern area, middle area and northern area was 34.1 °C, 28.8 °C, 31.8 °C and 30.4 °C, respectively. In the winter, the above four soil temperature indices showed that there was no significant difference in soil temperature between the middle and northern areas of the OAVS, and the relationship of soil temperature between the four areas was as follows: open field > southern area > middle area ≈ northern area. Taking the average

daytime soil temperature as an example, the soil temperature in the above four areas was 6.3 °C, 3.7 °C, 3.3 °C and 3.3 °C, respectively.

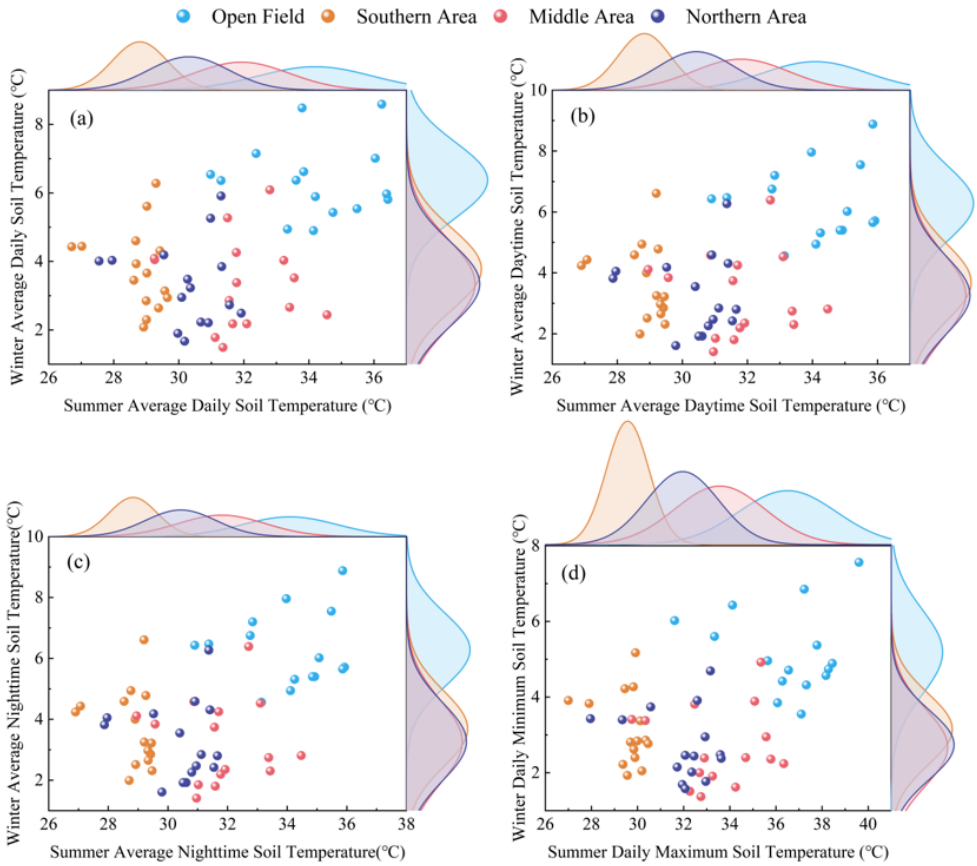

Figure 11. Marginal distribution curve data graph of soil temperature in summer and winter; (**a**) average daily soil temperature; (**b**) average daytime soil temperature; (**c**) average nighttime soil temperature; (**d**) daily extreme soil temperature.

3.2. Validation of ECOTECT Simulation

In order to verify the correctness and reliability of the calculated results of the established OAVS simulation model, combined with the previous test results, the measured values of each measurement point in the OAVS were compared with the simulated values. As Autodesk Ecotect Analysis 2011 is a simulation software based on the mean value of meteorological data for many years in the past, in order to avoid differences between the measured solar radiation intensity (E_m) and the average solar radiation intensity for many years, the average daylighting rate (R) was adopted for verification in this paper. The average daylighting rate ($R_{s\text{-}avg}$) and relative error (RE) obtained by simulation were calculated according to Equations (3) and (4).

$$R_{s\text{-}avg} = E_{s\text{-}in} / E_{s\text{-}out} \quad (3)$$

$$E = \left(R_{s\text{-}avg} - R_{m\text{-}avg}\right) / R_{m\text{-}avg} \quad (4)$$

where $E_{s\text{-}in}$ is the simulated value of the solar radiation intensity at the measuring point inside of the OAVS [MJ/(m^2·d)], $E_{s\text{-}out}$ is the simulated value of the solar radiation intensity at the measuring point outside of the OAVS [MJ/(m^2·d)] and $R_{s\text{-}avg}$ is the simulated value of the average daylighting rate (%).

Table 2 shows the comparison results between the measured values and simulated values. The measured values of each measurement point are in good agreement with the

simulated values, and the RE between them are all less than 10%. The simulation results are relatively reliable, indicating that the established OAVS model meets the simulation requirements and can be used for subsequent simulation studies.

Table 2. Comparison between simulated and measured R at each measuring point.

Season(s)	Area(s)	Measured Value/%	Simulated Value/%	Relative Error/%
Summer	Southern area	20.5	22.1	7.8
	Middle area	66.6	60.8	−8.7
	Northern area	22.7	21.0	−7.5
Winter	Southern area	26.4	28.6	8.3
	Middle area	24.7	25.5	3.2
	Northern area	19.7	18.2	−2.5

3.3. Results of OAVS Light Environment Simulation Analysis

3.3.1. Average Daily Solar Radiation

Figure 12 shows the distribution of ™average daily solar radiation intensity in the north–south direction right below the OAVS PV panel and between the two adjacent PV panels. It can be seen from the figure that the average daily radiation intensity inside the OAVS has an obvious gradient change. In the summer, the intensity in the north and south areas was low and the intensity in middle area was high. In winter, the intensity in the southern area was high, while the intensity in the other two areas was low.

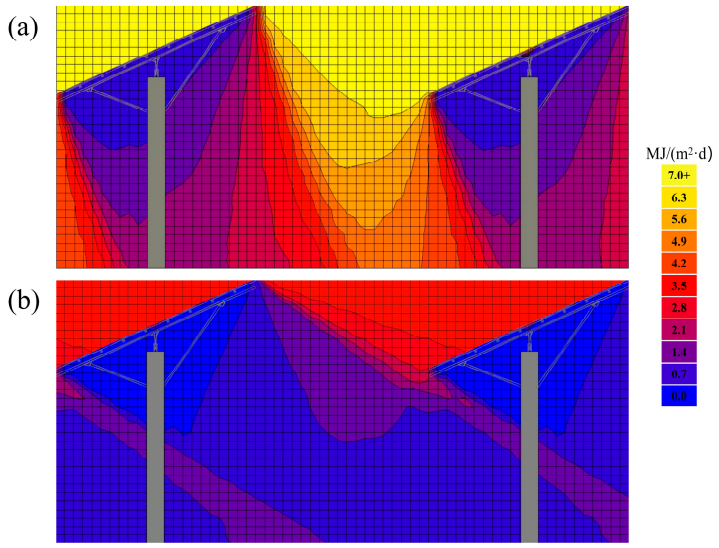

Figure 12. Cloud images of average daily solar intensity; (**a**) simulated cloud image in summer; (**b**) simulated cloud image in winter.

Figure 12a shows that the average daily radiation intensity in the canopy and below areas of the OAVS was between 1.88 and 5.58 MJ/(m^2·d) in the summer. The average daily radiation intensity in the southern, middle and northern areas was 1.94~2.72, 2.72~5.58 and 1.88~4.76 MJ/(m^2·d), respectively. On the whole, the average daily radiation intensity of the three internal areas was the highest in the middle area, and the average daily radiation intensity of the northern area of the middle area was greater, but there was no significant difference between the other two areas. Figure 12b shows that the average daily radiation intensity in the canopy and below areas of the OAVS that were not affected by side light was between 0.68 and 1.40 MJ/(m^2·d), and the overall average daily radiation intensity was small in the winter. The average daily radiation intensity in the southern, middle and northern areas was 0.73~1.40, 0.80~1.78 and 0.68~0.81 MJ/m^2·d), respectively. On

the whole, the southern area had the highest daily average radiation intensity of the three internal areas, while the other two areas had no significant difference.

3.3.2. Average Daily Sunshine Hours

Figure 13 shows the distribution of the average daily sunshine hours in the north–south direction right below the PV panel of the OAVS and between the two adjacent PV panels. On the whole, the variation rule is similar to the average daily solar radiation. It can be seen from the figure that the average daily sunshine duration inside of the OAVS had an obvious gradient change. On the whole, the OAVS in the summer showed a rule of short duration in the northern and southern areas and long duration in the middle area. In the winter, the OAVS showed a pattern of slightly longer duration in the southern area and shorter duration in the other two areas.

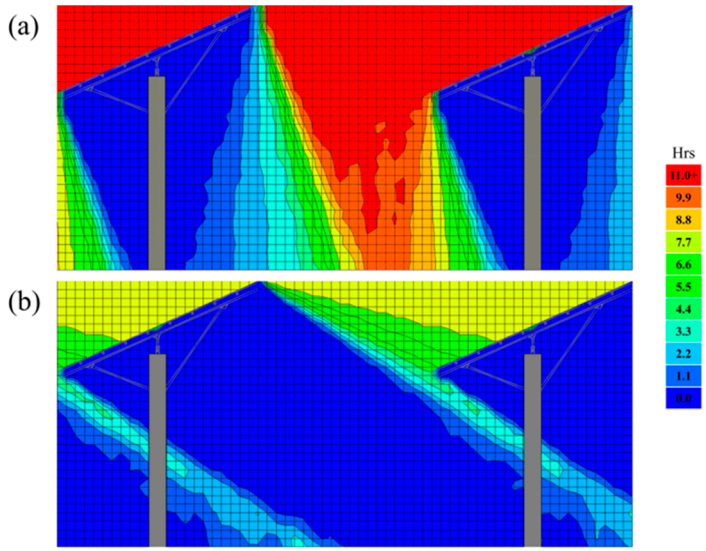

Figure 13. Cloud images of average daily sunshine hours; (**a**) simulated cloud image in summer; (**b**) simulated cloud image in winter.

Figure 13a shows that the average daily sunshine duration in the OAVS was between 0.10 and 11.12 h in the areas below the crop canopy and unaffected by side light in the summer. The average daily sunshine duration in the southern, middle and northern areas was 0.78~2.57 h, 2.57~11.12 h and 0.10~9.27 h, respectively. In general, the average daily sunshine hours of the three internal areas were the largest in middle area, and the average daily sunshine hours in the northern part of the middle area were greater, while there was no significant difference between the other two areas. Figure 13b shows that the average daily sunshine hours of the crop canopy and the areas below the OAVS that were not affected by side light ranged from 0.00 to 2.72 h, and the overall average daily sunshine hours were small in the winter. Among them, the average daily sunshine hours in the southern, middle and northern areas are 0.00~2.72, 0.00~2.64 and 0.00~0.55 h, respectively. On the whole, the southern area had the largest average daily sunshine hours, while the other two areas had no significant difference.

3.3.3. Average Daily Shading Rate

The variation in solar radiation intensity in the OAVS caused by the shading of the PV panel obviously affects the microecological environment of the system, and the shading rate (S) can be used to characterize the shading rate of the PV panel on the solar radiation intensity of the crop canopy or ground. The internal shading rate of the OAVS was calculated according to Equation (5), where the sum of the shading and lighting rate is 1.

$$S = (E_{s\text{-}out} - E_{s\text{-}in}) / E_{s\text{-}out} \quad (5)$$

Figure 14 shows the distribution of the average daily shading rate in the summer and winter in the north–south direction directly below the OAVS PV panel and between the two adjacent PV panels. It can be seen that there was an obvious gradient change in the internal shading rate of the OAVS. In the summer, the shading rate in the northern and southern areas was large, while the shading rate in the middle was small. In the winter, the shading rate in the southern area was small, while the shading rate in the other two areas was large.

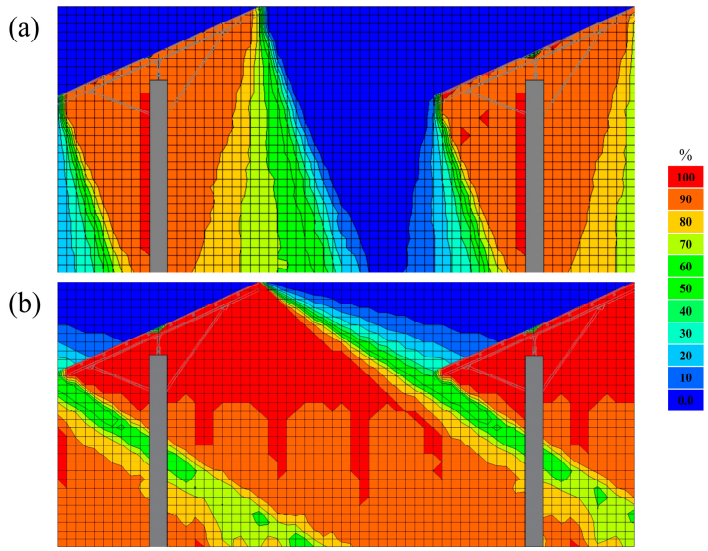

Figure 14. Cloud images of average daily shading rate; (**a**) simulated cloud image in summer; (**b**) simulated cloud image in winter.

Figure 14a shows that the shading rate of the canopy and the area below the crop in the OAVS which was not affected by side light ranged from 3.3% to 100% in the summer. Among them, the shading rate of the southern area was 77.6%~92.4%; the shading rate of the middle area was between 3.1% and 77.6% and the shading in the northern area was between 20.6% and 100%. On the whole, the southern area had the largest shading rate among the three interior areas, while the other two areas had no significant difference. Combined with agricultural production, the northern part of the middle area is more suitable for the growth of non-shade tolerant crops. Figure 14b shows that the shading rate of the OAVS which was not affected by side light ranged from 63.9% to 100%, and the overall shading rate was large in the winter. Among them, the shading rate of are area was 69.4%~100%; the shading rate in the middle area was 69.4%~100% and the shading in the northern area was 93.0%~100%. On the whole, the southern area was the least shaded among the three internal areas, while the other two areas had no significant difference.

4. Discussion

4.1. Temporal Variation in Light Environment in OAVS

For the OAVS, PV panels are an important factor affecting the light factor and have a significant impact on the agrivoltaic environment. The intensity of solar radiation is strongest at noon, weakest in the morning and evening and reaches its maximum around 12:00 noon. In addition, the solar radiation intensity is also affected by the weather and clouds. The variation in the solar radiation intensity fluctuates obviously on cloudy days, and the solar radiation intensity is significantly higher on sunny days than on cloudy days due to the influence of cloud thickness.

In the temperate regions of the northern hemisphere, the sunlight is strongest in the summer and weakest in the winter. The length of day and night is also different due to the change in the sun's height, and the solar radiation intensity changes periodically with the seasonal changes. Overall, OAVS PV panels have a significant impact on the interior light environment. In the summer, the lighting rate in the northern and southern areas

is only about 20% of that in the open field, while in the middle area, it can reach about 65%. Winter is relatively small, only about 20% in three areas. The solar altitude angle in eastern China is low in the winter, and the solar radiation intensity inside the system is relatively weak, while the opposite is true in the summer. Our results support previous findings that the AVS has a cooling function [41] but has a large impact on daylighting capacity and thus agricultural production effectiveness (PV + kiwifruit [42], PV + coffee [43], PV + potato [14]). In conclusion, the effectiveness of the OAVS in reducing solar radiation intensity level depends on the time of day and solar angle under the condition of a certain spatial structure and shape.

4.2. Spatial Variation in Light Environment in OAVS

According to experiment and simulation results, the spatial light environment of the OAVS is similar to that of the forest light environment [44]. Because PV panels strongly consume light availability and produce a strong vertical light environment gradient, this vertical light environment gradient has an important impact on the light competition of crops under PV panels, and thus affects the growth of crops. Taking the middle area as an example, the higher the height, the higher the photosynthetic activity of crops, the better the ability to use bright light; the photosynthetic activity of crops in the middle and bottom of the canopy is low, but the ability to adapt to low light is strong. The vertical gradient light environment in the southern and northern areas is opposite to that in the middle area. The higher the height, the less suitable for crop growth.

On the horizontal gradient, due to the influence of the PV panel spatial structure, solar altitude angle and other factors, as well as the difference in surface roughness and terrain height caused by precipitation, the acceptance of solar radiation on the surface varies greatly. Our research results show that the OAVS can reduce air temperature and soil temperature to a certain extent, mainly because the PV panel shading reduces the solar radiation received by the ground and the solar radiation temperature, so that the air temperature and soil temperature are reduced to a certain extent. Our findings are consistent with many previous studies on the effect of shading structure on temperature. For example, Middel et al. found that different building shadows could reduce the daytime solar radiation temperature by more than 17 °C [45].

4.3. Limitations and Future Research Directions of This Study

The study has several limitations. Firstly, the authors only studied the influence of continuously laid PV panels on the internal photothermal environment of the OAVS under a certain span and height. Expanding the test scope to OAVS with different photovoltaic panel laying densities, photovoltaic array spans and heights will produce different photothermal environments, which will have a different guiding significance for agricultural production, and also contribute to the standardization of the photovoltaic agricultural industry. At present, there are few OAVS with different spatial structure forms, which will be realized by transforming existing OAVS in the later stage.

This paper only analyzed the photothermal environment and did not establish the response mechanism of agricultural production to the environment based on the environment. In the follow-up study, environmental analysis and agricultural production can be combined to explore further.

The meteorological data imported in Autodesk Ecotect Analysis 2011 are the average data of nearly 30 years, so there are some differences between the simulated data and the data of the year of the environmental test. Another limitation is that the software takes a long time to compute.

5. Conclusions

The $R_{m\text{-}avg}$ in the middle area was 66.6% in the summer, while the $R_{m\text{-}avg}$ in the other two areas was about 20%. In the winter, the light environment in the southern area was slightly better, and the $R_{m\text{-}avg}$ can reach 26.4%, while the $R_{m\text{-}avg}$ in the three areas was

maintained at about 20%. The variation in the thermal environment in three areas was consistent with that in the light environment. The thermal environment of the OAVS middle area in the summer was better than that of the other two areas. The thermal environment of the southern area was better than that of the other two areas in the winter.

The OAVS optical environment model in eastern China was established, and the Simulated values were basically consistent with the experimental values at each test point, with the relative error within 10%. The constructed OAVS optical environment model can reflect the distribution of the optical environment factors in the OAVS. The simulation results show that the effectiveness of the OAVS in reducing the solar radiation intensity depends on the time of day and the solar angle. On the spatial scale, because the PV panels strongly consume the availability of light, the system produces a strong horizontal and vertical gradient of light environment.

The experimental method and simulation model can be applied to other regions of different latitudes and longitudes and specific climate conditions, so as to use the measured and simulated data to guide existing agricultural production. At the same time, using the simulation model, the optical performance of the photovoltaic agricultural system with a new structure can be obtained, so as to further guide the architectural design and agricultural production of the photovoltaic agricultural system.

Considering the effect of the OAVS agricultural production, the system's reasonable daylighting capacity is of great significance in engineering design. Because the power generation benefit is far greater than the agricultural production benefit, problems such as the optimal laying density of PV panels have not been solved. Therefore, this study can be used as a reference for further research on optimal PV panels laying density.

Author Contributions: Conceptualization, E.B. and C.W.; Methodology, L.Z. and C.W.; Software, Z.Y. and X.W.; Validation, Z.Y.; Formal analysis, Z.Y. and X.W.; Investigation, L.Z., W.W. and C.W.; Resources, C.Y.; Data curation, L.Z. and G.X.; Writing—original draft, L.Z. and G.X.; Writing—review and editing, W.W., X.W. and C.W.; Visualization, Z.Y. and C.Y.; Supervision, C.Y. and E.B.; Project administration, E.B.; Funding acquisition, E.B. All authors have read and agreed to the published version of the manuscript.

Funding: This research was funded by Key Laboratory of Farm Building in Structure and Construction, Ministry of Agriculture and Rural Affairs, China (202103).

Data Availability Statement: The data presented in this study are available upon request from the corresponding author.

Conflicts of Interest: The authors declare no conflict of interest.

References

1. Xue, J.L. Photovoltaic agriculture—New opportunity for photovoltaic applications in China. *Renew. Sustain. Energy Rev.* **2017**, *73*, 1–9. [CrossRef]
2. Muñoz-García, M.A.; Hernández-Callejo, L. Photovoltaics and electrification in agriculture. *Agronomy* **2021**, *12*, 44. [CrossRef]
3. Havrysh, V.; Kalinichenko, A.; Szafranek, E.; Hruban, V. Agricultural land: Crop production or photovoltaic power plants. *Sustainability* **2022**, *14*, 5099. [CrossRef]
4. Sarr, A.; Soro, Y.M.; Tossa, A.K.; Diop, L. Agrivoltaic, a synergistic co-location of agricultural and energy production in perpetual mutation: A comprehensive review. *Processes* **2023**, *11*, 948. [CrossRef]
5. Zhou, W.D.; Zhuang, G.Y.; Liu, L.B. Comprehensive assessment of energy supply-side and demand-side coordination on pathways to carbon neutrality of the yangtze river delta in China. *J. Clean. Prod.* **2023**, *404*, 136904. [CrossRef]
6. Miao, Q.Q.; Shi, C.Y.; Zhang, X.P. Photovoltaic technology under carbon neutrality. *Huagong Jinzhan* **2022**, *41*, 1125–1131.
7. Jing, R.; He, Y.; He, J.J.; Liu, Y.; Yang, S.B. Global sensitivity based prioritizing the parametric uncertainties in economic analysis when co-locating photovoltaic with agriculture and aquaculture in China. *Renew. Energy* **2022**, *194*, 1048–1059. [CrossRef]
8. China's Photovoltaic Power Generation Construction and Operation in 2022. Available online: http://www.nea.gov.cn/2023-02/17/c_1310698128.htm (accessed on 12 June 2023).
9. Wang, W.Y.; Zang, M.W.; Zhang, H.; Bai, Y.C.; Li, J.H.; Wang, D.Y.; Yuan, K.; Li, D. Current status of and development suggestions for food science and technology innovation power layout in China. *Sci. Food* **2022**, *43*, 336–341.
10. Dinesh, H.; Pearce, J.M. The potential of agrivoltaic systems. *Renew. Sustain. Energy Rev.* **2016**, *54*, 299–308. [CrossRef]

11. Geng, S.Q.; Wang, L. Planning of qianyan modern photovoltaic agricultural demonstration park basing on the photovoltaic model of medicinal materials. *Tianjin Agric. Sci.* **2021**, *27*, 75–79.
12. Campana, P.E.; Stridh, B.; Amaducci, S.; Colauzzi, M. Optimisation of vertically mounted agrivoltaic systems. *J. Clean. Prod.* **2021**, *325*, 129091. [CrossRef]
13. Kim, S.; Kim, S.; Yoon, C.Y. An efficient structure of an agrophotovoltaic system in a temperate climate region. *Agronomy* **2021**, *11*, 1584. [CrossRef]
14. Schulz, V.S.; Munz, S.; Stolzenburg, K.; Hartung, J.; Weisenburger, S.; Graeff-Hönninger, S. Impact of Different Shading Levels on Growth, Yield and Quality of Potato (*Solanum tuberosum* L.). *Agronomy* **2019**, *9*, 330. [CrossRef]
15. Edouard, S.; Combes, D.; Van Iseghem, M.; Tin, M.N.W.; Escobar-Gutierrez, A.J. Increasing land productivity with agriphotovoltaics: Application to an alfalfa field. *Appl. Energy* **2023**, *329*, 120207. [CrossRef]
16. Valle, B.; Simonneau, T.; Sourd, F.; Pechier, P.; Hamard, P.; Frisson, T.; Ryckewaert, M.; Christophe, A. Increasing the total productivity of a land by combining mobile photovoltaic panels and food crops. *Appl. Energy* **2017**, *206*, 1495–1507. [CrossRef]
17. Huang, K.; Shu, L.; Li, K.L.; Yang, F.; Han, G.J.; Wang, X.C.; Pearson, S. Photovoltaic agricultural internet of things towards realizing the next generation of smart farming. *IEEE Access* **2020**, *8*, 76300–76312. [CrossRef]
18. Leon, A.; Ishihara, K.N. Influence of allocation methods on the lc-co2 emission of an agrivoltaic system. *Resour. Conserv. Recy.* **2018**, *138*, 110–117. [CrossRef]
19. Hassanpour Adeh, E.; Selker, J.S.; Higgins, C.W. Remarkable agrivoltaic influence on soil moisture, micrometeorology and water-use efficiency. *PLoS ONE* **2018**, *13*, e0203256. [CrossRef]
20. Ali Abaker Omer, A.; Liu, W.; Li, M.; Zheng, J.; Zhang, F.; Zhang, X.; Osman Hamid Mohammed, S.; Fan, L.; Liu, Z.; Chen, F.; et al. Water evaporation reduction by the agrivoltaic systems development. *Sol. Energy* **2022**, *247*, 13–23. [CrossRef]
21. Feuerbacher, A.; Laub, M.; Högy, P.; Lippert, C.; Pataczek, L.; Schindele, S.; Wieck, C.; Zikeli, S. An analytical framework to estimate the economics and adoption potential of dual land-use systems: The case of agrivoltaics. *Agr. Syst.* **2021**, *192*, 103193. [CrossRef]
22. Giri, N.C.; Mohanty, R.C. Agrivoltaic system: Experimental analysis for enhancing land productivity and revenue of farmers. *Energy Sustain. Dev.* **2022**, *70*, 54–61. [CrossRef]
23. Chen, J.; Liu, Y.P.; Wang, L.J. Research on coupling coordination development for photovoltaic agriculture system in China. *Sustainability* **2019**, *11*, 1065. [CrossRef]
24. Li, Z.; Sun, X.; Zhou, J.W.; Wu, L.H.; Bi, D.; Zhao, J.; Zhu, R.F.; Christie, P. Sustainable phytoextraction of metal-polluted agricultural land used for commercial photovoltaic power generation. *J. Clean. Prod.* **2023**, *391*, 136093. [CrossRef]
25. Santra, P.; Meena, H.M.; Yadav, O.P. Spatial and temporal variation of photosynthetic photon flux density within agrivoltaic system in hot arid region of india. *Biosyst. Eng.* **2021**, *209*, 74–93. [CrossRef]
26. Marrou, H.; Guilioni, L.; Dufour, L.; Dupraz, C.; Wery, J. Microclimate under agrivoltaic systems: Is crop growth rate affected in the partial shade of solar panels? *Agric. For. Meteorol.* **2013**, *177*, 117–132. [CrossRef]
27. Gao, X.Q.; Yang, L.W.; Lyu, F.; Ma, L.Y.; Hui, X.Y.; Hou, X.Y.; Li, H.L. Observational study on the impact of the large solar farm on air temperature and humidity in desert areas of golmud. *Acta Energiae Solaris Sin.* **2016**, *37*, 2905–2919.
28. Chang, R.; Shen, Y.B.; Luo, Y.; Wang, B.; Yang, Z.B.; Guo, P. Observed surface radiation and temperature impacts from the large-scale deployment of photovoltaics in the barren area of gonghe, China. *Renew. Energy* **2018**, *118*, 131–137. [CrossRef]
29. Sailor, D.J.; Anand, J.; King, R.R. Photovoltaics in the built environment: A critical review. *Energy Build.* **2021**, *253*, 111479. [CrossRef]
30. Ezzaeri, K.; Fatnassi, H.; Bouharroud, R.; Gourdo, L.; Bazgaou, A.; Wifaya, A.; Demrati, H.; Bekkaoui, A.; Aharoune, A.; Poncet, C.; et al. The effect of photovoltaic panels on the microclimate and on the tomato production under photovoltaic canarian greenhouses. *Sol. Energy* **2018**, *173*, 1126–1134. [CrossRef]
31. Ayoub, M.; Elseragy, A. Parameterization of traditional domed-roofs insolation in hot-arid climates in aswan, Egypt. *Energy Environ.* **2017**, *29*, 109–130. [CrossRef]
32. Wu, Q.; Jo, H.K. A study on ecotect application of local climate at a residential area in chuncheon, korea. *J. Environ. Eng. Landsc.* **2015**, *23*, 94–101. [CrossRef]
33. Yang, L.; He, B.J.; Ye, M. Application research of ecotect in residential estate planning. *Energy Build.* **2014**, *72*, 195–202. [CrossRef]
34. Akbari, H.; Cherati, S.M.; Monazam, N.H.; Noguchi, M. Effect of courtyards' geometrical parameters on climate adaptability and shading performance in hot-arid climate of yazd (Iran). *Sustain. Energy Technol. Assess.* **2021**, *48*, 101594. [CrossRef]
35. Li, H.L.; Wu, D.; Zhou, J.Z. Effects of tubular daylight guidance systems on the daylighting performance and energy savings in office buildings under different climate zones. *J. Renew. Sustain. Energy* **2021**, *13*, 065102. [CrossRef]
36. Ahriz, A.; Mesloub, A.; Djeffal, L.; Alsolami, B.M.; Ghosh, A.; Abdelhafez, M.H.H. The use of double-skin façades to improve the energy consumption of high-rise office buildings in a mediterranean climate (csa). *Sustainability* **2022**, *14*, 6004. [CrossRef]
37. He, D.S.; Chang, J.G.; Han, X. Direct radiation model of louver shading in office building shade based on network optimization method. *Comput. Intell. Neurosci.* **2022**, *2022*, 5766448. [CrossRef]
38. Chi, F.A.; Borys, I.; Jin, L.; Zhu, Z.Z.; Bart, D. The strategies and effectiveness of climate adaptation for the thousand pillars dwelling based on passive elements and passive spaces. *Energy Build.* **2019**, *183*, 17–44. [CrossRef]
39. Iommi, M. Daylighting performances and visual comfort in le corbusier's architecture. The daylighting analysis of seven unrealized residential buildings. *Energy Build.* **2019**, *184*, 242–263. [CrossRef]

40. Sun, Z.P.; Huang, W.Y.; Li, T.L.; Tong, X.J.; Bai, Y.K.; Ma, J. Light and temperature performance of energy-saving solar greenhouse assembled with color plate. *Trans. Chin. Soc. Agric. Eng.* **2013**, *29*, 159–167.
41. Cho, J.; Park, S.M.; Park, A.R.; Lee, O.C.; Nam, G.; Ra, I.H. Application of photovoltaic systems for agriculture: A study on the relationship between power generation and farming for the improvement of photovoltaic applications in agriculture. *Energies* **2020**, *13*, 4815. [CrossRef]
42. Jiang, S.; Tang, D.; Zhao, L.; Liang, C.; Cui, N.; Gong, D.; Wang, Y.; Feng, Y.; Hu, X.; Peng, Y. Effects of different photovoltaic shading levels on kiwifruit growth, yield and water productivity under "agrivoltaic" system in southwest China. *Agric. Water Manag.* **2022**, *269*, 107675. [CrossRef]
43. Assis, B.D.P.; Gross, E.; Pereira, N.E.; Mielke, M.S.; Júnior, G.A.G. Growth response of four conilon coffee varieties (Coffea canephora Pierre ex A. Froehner) to different shading levels. *J. Agric. Sci.* **2019**, *11*, 29. [CrossRef]
44. Song, Y.; Ryu, Y. Seasonal changes in vertical canopy structure in a temperate broadleaved forest in korea. *Ecol. Res.* **2015**, *30*, 821–831. [CrossRef]
45. Middel, A.; Alkhaled, S.; Schneider, F.A.; Hagen, B.; Coseo, P. 50 grades of shade. *Bull. Am. Meteorol. Soc.* **2021**, *102*, E1805–E1820. [CrossRef]